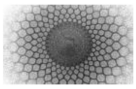
TTMP vol 3 (4), 2026
doi: 10.30511/TTMP.2026.2107007.1098

Transactions in Theoretical and Mathematical Physics



Tunable Casimir Torque in a Heterogeneous Rotational Microsystem Using Phase-Change Materials

Zahra Rabiee[1,a], **Fatemeh Tajik**[1]

[1]Department of Condensed Matter Physics, Faculty of Physics, Alzahra University, Tehran, Iran

Received: 25 September 2026 / Accepted: 28 October 2026 / Published: 05 November 2026

Abstract This study investigates the Casimir torque in a rotational microelectromechanical system (MEMS) with heterogeneous surface coatings using Lifshitz theory in conjunction with the proximity force approximation (PFA). The system consists of two parallel plates: a stationary, highly electrically conductive gold plate and a movable plate that rotates about its central axis. The movable plate is divided into two regions with different surface coatings: the left half in the schematic is coated with silicon carbide (SiC), whereas the right half is coated with a phase-change material (PCM), considered in both its crystalline and amorphous phases. We assume an equilibrium separation of 300 nm between the plates in the parallel configuration and consider small rotational angles. The results show that switching the PCM coating from the amorphous to the crystalline phase increases the net Casimir torque by approximately a factor of 12 at a normalized rotation angle of $\phi = 0.9$. Thermal fluctuations at 450 K further enhance the torque; however, in the crystalline phase, the temperature dependence becomes less pronounced because quantum fluctuations dominate. The equivalent Casimir voltage required to counteract the Casimir torque with an electrostatic torque in the realistic material configuration is substantially lower than that for an ideal, perfectly conducting system. These results demonstrate that the proposed heterogeneous rotational system may provide a viable platform for active optomechanical switching and tunable thermal sensing in NEMS applications.

Keywords: Optical properties; Silicon carbide; Casimir torque; Phase change material; Micro electromechanical system; Lifshitz theory; Casimir force.

1 Introduction

The Casimir force, predicted by Hendrik Casimir in 1948, originates from quantum fluctuations of the electromagnetic field in vacuum [1]. At submicron separations, this interaction increases rapidly and can induce irreversible stiction between components, thereby compromising the functionality and reliability of micro- and nanoelectromechanical systems (MEMS/NEMS) [2, 7]. Consequently, developing effective strategies to control and tune Casimir interactions is of considerable practical importance.

One promising approach uses phase-change materials (PCMs), which can reversibly switch between ordered crystalline and disordered amorphous phases in response to thermal or electrical stimuli. Depending on the material, this phase transition can substantially change the optical response, particularly the frequency-dependent dielectric function [3, 4]. Previous studies have demonstrated that these changes can modulate the Casimir force and affect the actuation dynamics of microsystems [3, 4]. More broadly, recent reviews discuss the influence of material optical re-

[a]Corresponding author: rabiee2213@gmail.com

sponse, geometry, temperature, conductivity, and surface morphology on Casimir interactions and their applications in MEMS [8, 9].

In this work, we investigate a two-segment rotational microsystem in which the movable plate comprises two regions coated with different materials: silicon carbide (SiC) and a phase-change material (PCM). The primary objective is to calculate the net Casimir torque arising from the system's optical heterogeneity and to investigate how phase transitions and finite temperature affect the torque magnitude and the corresponding electrostatic-equivalent voltage. Our approach combines mechanical rotation, material heterogeneity, phase switching, and thermal effects within the framework of Lifshitz theory and the proximity force approximation (PFA). Recent theoretical work has also highlighted the relevance of thermal effects to Casimir torque between birefringent plates [11]. Here, we examine thermal effects in a heterogeneous rotational geometry, with particular emphasis on the influence of the PCM phase on the net torque and its temperature dependence. A closely related study investigated phase transitions and thermal fluctuations in nonhomogeneous torsional Casimir MEMS containing SiC and a PCM [12]. The present treatment focuses on the equilibrium torque and electrostatic-equivalent voltage.

2 System Geometry and Calculation Method

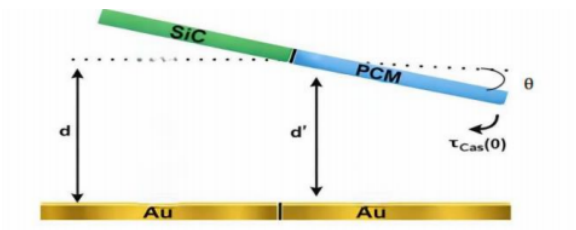


Fig. 1 Schematic of the rotational system consisting of a stationary gold plate and a movable plate with SiC coating on the left half and PCM coating on the right half. Positive rotation lowers the PCM side toward the stationary plate.

The system consists of a stationary bottom plate made of gold (Au) and a movable top plate with a total length $L_x = 2\times10^{-5}\,\mathrm{m}$ and a width $L_y = 10^{-5}\,\mathrm{m}$. As shown in Fig. 1, the left half of the movable plate is coated with silicon carbide (SiC), whereas the right half is coated with a phase-change material (PCM), considered in both its crystalline and amorphous phases. The PCM investigated here is silver–indium–antimony–telluride (Ag–In–Sb–Te, AIST).

The initial separation between the two plates in the parallel configuration is $d = 300\,\mathrm{nm}$. The movable plate can rotate through a small angle θ about its central axis. For a positive rotation that brings the PCM-coated side closer to the gold plate, the local separations at a distance r from the rotation axis are

$$d'_L = d + r\sin\theta, \qquad d'_R = d - r\sin\theta. \tag{1}$$

Both the material heterogeneity and the rotational displacement can contribute to a net Casimir torque about the rotation axis.

According to Lifshitz theory, the magnitude of the attractive Casimir pressure between two parallel, nonmagnetic plates separated by a vacuum gap h at temperature T is [5]

$$p(h,T) = \frac{k_\mathrm{B}T}{\pi}{\sum_{n=0}^{\infty}}' \int_0^\infty k_\parallel \,\mathrm{d}k_\parallel\, q_n \times \sum_{\nu=\mathrm{TE,TM}} \frac{r_{1\nu}r_{2\nu}e^{-2q_nh}}{1-r_{1\nu}r_{2\nu}e^{-2q_nh}}. \tag{2}$$

Here, the prime indicates that the $n=0$ term has half weight. The Matsubara frequencies and perpendicular wave-vector components are defined by

$$\xi_n = \frac{2\pi k_\mathrm{B}T}{\hbar}n, \tag{3}$$

$$q_n = \sqrt{k_\parallel^2 + \frac{\xi_n^2}{c^2}}, \tag{4}$$

$$\kappa_{i,n} = \sqrt{k_\parallel^2 + \varepsilon_i(i\xi_n)\frac{\xi_n^2}{c^2}}. \tag{5}$$

The vacuum relative permittivity is unity. The Fresnel reflection coefficients at the vacuum–material interfaces are

$$r_{i,\mathrm{TE}} = \frac{q_n - \kappa_{i,n}}{q_n + \kappa_{i,n}}, \tag{6}$$

$$r_{i,\mathrm{TM}} = \frac{\varepsilon_i(i\xi_n)q_n - \kappa_{i,n}}{\varepsilon_i(i\xi_n)q_n + \kappa_{i,n}}. \tag{7}$$

All reflection coefficients in Eq. (2) are evaluated at $i\xi_n$ and $k_\parallel$.

The dielectric functions at imaginary frequencies are obtained from the measured optical response through

$$\varepsilon_j(i\xi) = 1 + \frac{2}{\pi}\int_0^\infty \frac{\omega\,\mathrm{Im}\,\varepsilon_j(\omega)}{\omega^2+\xi^2}\,\mathrm{d}\omega. \tag{8}$$

Experimental optical data are supplemented, where appropriate, by a Drude extrapolation at low frequencies [4, 7]. The Drude dielectric function on the imaginary frequency axis is

$$\varepsilon_{\mathrm{D}}(i\xi) = 1 + \frac{\omega_{\mathrm{p}}^2}{\xi(\xi+\gamma)}, \tag{9}$$

where ω_{p} is the plasma frequency and γ is the relaxation rate. At zero temperature, the Matsubara sum is replaced by a continuous frequency integral:

$$k_{\mathrm{B}}T\sum_{n=0}^{\infty}{}' \longrightarrow \frac{\hbar}{2\pi}\int_0^\infty \mathrm{d}\xi. \tag{10}$$

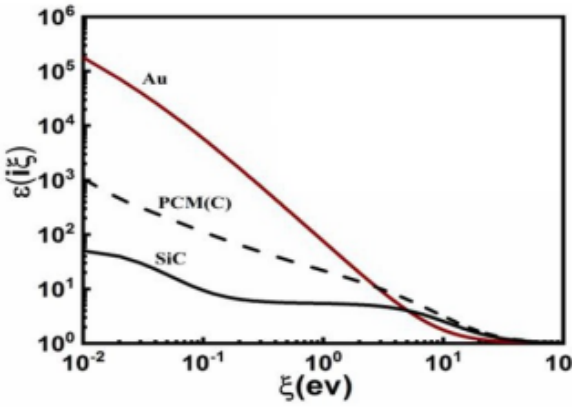


Fig. 2 Dielectric functions $\varepsilon(i\xi)$ as a function of imaginary frequency for Au, SiC, and crystalline PCM, denoted by PCM(C), used in the rotational MEMS.

For small rotational angles and gaps much smaller than the lateral plate dimensions, we employ the proximity force approximation (PFA) [6]. Let $a = L_x/2$, and choose a signed coordinate x along the movable plate such that the PCM occupies $0 < x < a$ and SiC occupies $-a < x < 0$. Positive rotation reduces the gap on the PCM side. Within the linearized small-angle geometry, the local separation is

$$h(x,\theta) = d - x\theta. \tag{11}$$

We denote by $p_j(h,T) > 0$ the magnitude of the attractive Lifshitz pressure between gold and material j at separation h and temperature T. Taking positive torque to increase θ, the local proximity approximation gives

$$\tau_{\mathrm{Cas}}(\theta,T) = L_y\int_0^a x\Big[p_{\mathrm{PCM}}(d-x\theta,T) - p_{\mathrm{SiC}}(d+x\theta,T)\Big]\,\mathrm{d}x. \tag{12}$$

This expression follows by integrating the local attractive force with its signed moment arm about the central axis.

Equivalently, let $\mathscr{F}_j(h,T)$ denote the interaction free energy per unit area, normalized to vanish at infinite separation. With the positive attractive-pressure convention,

$$p_j(h,T) = \frac{\partial\mathscr{F}_j(h,T)}{\partial h}. \tag{13}$$

The interaction free energy in the same approximation is

$$U_{\mathrm{Cas}}(\theta,T) = L_y\int_0^a\Big[\mathscr{F}_{\mathrm{PCM}}(d-x\theta,T) + \mathscr{F}_{\mathrm{SiC}}(d+x\theta,T)\Big]\,\mathrm{d}x. \tag{14}$$

The relation

$$\tau_{\mathrm{Cas}} = -\frac{\partial U_{\mathrm{Cas}}}{\partial\theta} \tag{15}$$

then reproduces Eq. (12).

For smooth pressure functions and $a|\theta|/d \ll 1$, Taylor expansion yields

$$\tau_{\mathrm{Cas}}(\theta,T) = \tau_0(T) + K_{\mathrm{Cas}}(T)\theta + \mathscr{O}(\theta^2), \tag{16}$$

where

$$\tau_0(T) = \frac{L_y a^2}{2}\left[p_{\mathrm{PCM}}(d,T) - p_{\mathrm{SiC}}(d,T)\right], \tag{17}$$

and

$$K_{\mathrm{Cas}}(T) = -\frac{L_y a^3}{3}\left[\frac{\partial p_{\mathrm{PCM}}(d,T)}{\partial d} + \frac{\partial p_{\mathrm{SiC}}(d,T)}{\partial d}\right]. \tag{18}$$

The constant term measures the torque caused by material heterogeneity in the parallel configuration, whereas the linear coefficient measures the angular response. For identical coatings, $\tau_0 = 0$, and the torque is an odd function of θ. For heterogeneous coatings, a nonzero torque may already be present at $\theta = 0$.

Within the linearized geometry, we define

$$\theta_0 = \frac{d}{a}, \qquad \phi = \frac{\theta}{\theta_0}. \tag{19}$$

For $|\phi| < 1$, the smallest and largest local gaps are

$$h_{\min} = d(1 - |\phi|), \tag{20}$$

$$h_{\max} = d(1 + |\phi|). \tag{21}$$

Using $d = 300\,\text{nm}$ and $a = 10\,\mu\text{m}$, we obtain $\theta_0 = 0.03\,\text{rad}$. Thus, $\phi = 0.9$ corresponds to $\theta = 0.027\,\text{rad}$ and a minimum gap of 30 nm. A normalized angle close to unity therefore represents proximity to contact, even though the physical angle remains small.

The Taylor expansion in Eq. (16) requires $|\phi| \ll 1$ and should not be extrapolated to the near-contact regime. The validity of the local proximity approximation is a separate issue involving the gap, slope, finite plate dimensions, and coating boundary. Near contact, the results can also become more sensitive to surface roughness and the material description at small separations.

3 Results

3.1 Casimir Torque at Zero Temperature

Table 1 Casimir torque at zero temperature, expressed in units of $10^{-15}\,\text{N m}$.

Normalized angle ϕ	Ideal	Crystalline	Amorphous
0.01	0.87	0.81	0.53
0.30	1.14	0.98	0.61
0.50	2.74	1.95	0.84
0.80	16.9	7.2	1.3
0.90	135.5	34.8	2.9

Table 1 presents the Casimir torque for the ideal perfectly conducting case and the realistic material configuration as a function of the normalized rotation angle,

$$\phi = \frac{\theta}{\theta_0} = \frac{a\theta}{d}, \qquad a = \frac{L_x}{2}. \tag{22}$$

In the crystalline phase, the torque is closer to the ideal perfectly conducting value than in the amorphous phase, particularly at small normalized angles. The amorphous phase produces a substantially smaller torque. At $\phi = 0.9$, the crystalline-phase torque exceeds the amorphous-phase torque by a factor of approximately 12.

3.2 Effect of Temperature

Figures 3 and 4 show the torque reduction factor,

$$\eta(\phi, T) = \frac{\tau_{\text{Cas}}(\phi, T)}{\tau_{\text{Cas}}^{\text{ID}}(\phi, T)}, \tag{23}$$

where $\tau_{\text{Cas}}^{\text{ID}}$ denotes the torque for the ideal perfectly conducting reference system at the same angle and temperature. The reduction factor increases at 450 K compared with its zero-temperature value, particularly in the amorphous phase.

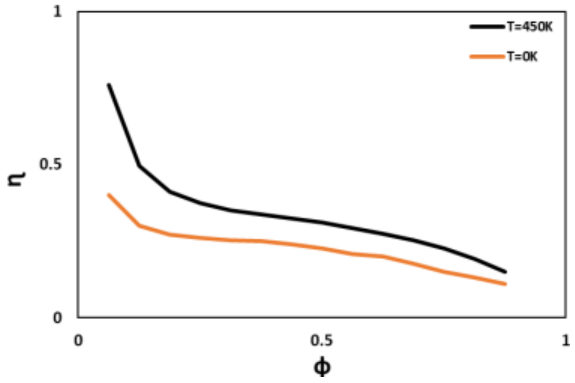


Fig. 3 Torque reduction factor $\eta = \tau_{\text{Cas}}/\tau_{\text{Cas}}^{\text{ID}}$ versus normalized angle ϕ for the microsystem containing amorphous PCM at $T = 0\,\text{K}$ and $T = 450\,\text{K}$.

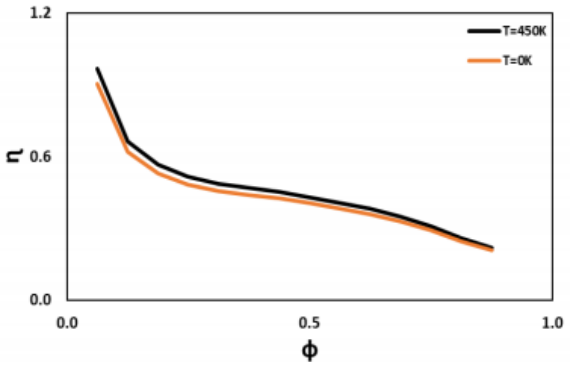


Fig. 4 Torque reduction factor $\eta = \tau_{\text{Cas}}/\tau_{\text{Cas}}^{\text{ID}}$ versus normalized angle ϕ for the microsystem containing crystalline PCM at $T = 0\,\text{K}$ and $T = 450\,\text{K}$.

The finite-temperature calculations at $T = 450\,\text{K}$ show that thermal fluctuations enhance the total Casimir torque. However, the magnitude of this enhancement strongly depends on the PCM phase. In the crystalline phase, where the

quantum contribution remains dominant, increasing the temperature produces only a modest change in the torque, with an enhancement of less than 20%. By contrast, in the amorphous phase, where the zero-temperature Casimir torque is comparatively weak, the thermal contribution can account for up to approximately 50% of the total torque.

This pronounced phase-dependent thermal response suggests two distinct operating regimes: a thermally responsive regime in the amorphous phase, potentially suitable for temperature sensing, and a comparatively thermally stable regime in the crystalline phase. Such phase-dependent tunability could benefit the development of adaptive NEMS devices intended to operate in environments with substantial temperature variations.

These observations are consistent with the broader literature showing that thermal corrections to Casimir interactions depend on geometry, separation, and material optical response [9, 10]. Recent theoretical work has also demonstrated substantial thermal effects on Casimir torque between birefringent plates [11]. A study of nonhomogeneous torsional PCM MEMS also reported reduced sensitivity of actuation to thermal fluctuations in the crystalline phase [12].

3.3 Equivalent Casimir Voltage

The compensating electrodes must produce a torque opposite to the Casimir torque. Their placement and electrical connection determine both the sign and magnitude of the electrostatic torque; coating heterogeneity alone does not specify this electrode configuration. For a specified electrode configuration, let $C(\theta)$ denote the capacitance. At a fixed applied voltage V, the electrostatic torque is

$$\tau_{\mathrm{el}}(\theta,V)=\frac{V^2}{2}\frac{\mathrm{d}C}{\mathrm{d}\theta}=G(\theta)V^2, \tag{24}$$

where

$$G(\theta)=\frac{1}{2}\frac{\mathrm{d}C}{\mathrm{d}\theta}. \tag{25}$$

The voltage producing an electrostatic torque equal in magnitude to the Casimir torque is

$$V_{\mathrm{eq}}(\theta,T)=\sqrt{\frac{|\tau_{\mathrm{Cas}}(\theta,T)|}{|G(\theta)|}}, \qquad G(\theta)\neq 0. \tag{26}$$

This magnitude comparison corresponds to actual torque compensation only when the two torques have opposite signs. In that case, the signed balance condition is

$$\tau_{\mathrm{Cas}}(\theta,T)+G(\theta)V^2=0, \tag{27}$$

which yields

$$V^2=-\frac{\tau_{\mathrm{Cas}}(\theta,T)}{G(\theta)}\geq 0. \tag{28}$$

At a fixed angle and for the same electrostatic geometry, the material and ideal-conductor calculations must therefore satisfy

$$\frac{V_{\mathrm{eq}}^{\mathrm{mat}}}{V_{\mathrm{eq}}^{\mathrm{ID}}}=\sqrt{\frac{|\tau_{\mathrm{Cas}}^{\mathrm{mat}}|}{|\tau_{\mathrm{Cas}}^{\mathrm{ID}}|}}. \tag{29}$$

This identity provides a direct consistency check between the torque and equivalent-voltage results. Torque balance alone does not establish stability. Stability additionally requires a negative derivative of the total torque with respect to angle at equilibrium, including any mechanical restoring torque:

$$\left.\frac{\partial\tau_{\mathrm{tot}}}{\partial\theta}\right|_{\theta=\theta_{\mathrm{eq}}}<0, \tag{30}$$

where the derivative is evaluated at fixed applied voltage and temperature, and

$$\tau_{\mathrm{tot}}=\tau_{\mathrm{Cas}}+\tau_{\mathrm{el}}+\tau_{\mathrm{mech}}. \tag{31}$$

For comparison, the closed-form ideal-conductor reference expression used in the original formulation is

$$V_{\mathrm{eq}}^{\mathrm{ID}}(\phi)=\left[\frac{\pi^2\hbar c}{90\varepsilon_0 d^2}\times\frac{\phi^3(3+\phi^2)}{(1-\phi^2)^3\left[\ln(1-\phi)+\frac{\phi}{1-\phi}\right]}\right]^{1/2}, \qquad 0<\phi<1. \tag{32}$$

Here, ε_0 denotes the vacuum permittivity in SI units, not the vacuum relative permittivity, which is unity. This expression is a zero-temperature ideal-conductor magnitude benchmark. Its electrostatic geometry factor is that of a single half-plate parallel-gap electrode with capacitance

$$C_{\mathrm{ref}}(\theta)=\frac{\varepsilon_0 L_y}{\theta}\ln\left(\frac{d}{d-a\theta}\right). \tag{33}$$

For positive θ, this electrode attracts the approaching half and gives a positive torque. It therefore does not, by itself, compensate a positive Casimir torque. Actual compensation requires an electrode arrangement with the opposite torque sign, using its own $G(\theta)$ in Eq. (26). The closed-form benchmark must not be applied to the realistic heterogeneous system without the appropriate material torque and electrode geometry.

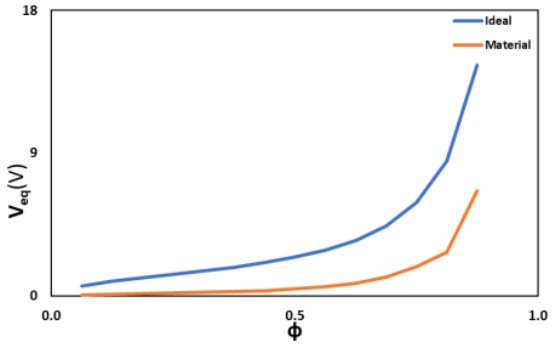


Fig. 5 Equivalent Casimir voltage V_{eq} versus normalized angle $\phi = \theta/\theta_0$ for the ideal perfectly conducting configuration and the realistic microsystem composed of crystalline PCM, SiC, and Au at $T = 0\,\mathrm{K}$.

The calculation of the equivalent Casimir voltage shows that the voltage required to counterbalance the Casimir torque through an electrostatic torque in the realistic material configuration is substantially lower than that required in the ideal perfectly conducting case. For example, for the same assumed electrostatic geometry at $\phi = 0.8$, the equivalent voltage is approximately $V_{\mathrm{eq}} = 2.74\,\mathrm{V}$ in the crystalline phase and $V_{\mathrm{eq}} = 1.16\,\mathrm{V}$ in the amorphous phase. The corresponding value for the ideal perfectly conducting configuration is $V_{\mathrm{eq}}^{\mathrm{ID}} = 4.2\,\mathrm{V}$.

The substantially reduced compensation voltage indicates that the Casimir-induced rotational behavior can be controlled using relatively low electrostatic bias voltages, potentially reducing the electrical energy required for actuation and control. In the amorphous phase, where the intrinsic Casimir torque is comparatively weak, only a small electrostatic bias is required to compensate for the interaction. Provided that the stability condition is also satisfied, this may allow operation near a zero-total-torque equilibrium. This characteristic may be advantageous for low-power memory and switching concepts in which minimal actuation energy and stable near-zero-torque states are desirable.

4 Conclusion

In this study, we investigated the net Casimir torque in a rotational microsystem with heterogeneous surface coatings of SiC and a phase-change material (PCM), using Lifshitz theory in conjunction with the proximity force approximation (PFA). The results show that switching the PCM from the amorphous to the crystalline phase substantially enhances the Casimir torque. At a normalized rotation angle of $\phi = 0.9$, the torque in the crystalline phase is approximately 12 times greater than that in the amorphous phase.

This pronounced difference primarily reflects the substantial change in the PCM's frequency-dependent dielectric response across the phase transition. In particular, the crystalline phase exhibits a stronger absorptive response, characterized by an enhanced imaginary part of the dielectric function over relevant frequency ranges, and consequently displays more metal-like optical behavior than the amorphous phase. This modification of the electromagnetic reflection properties alters the fluctuation-induced interaction within the gap, leading to a stronger Casimir interaction and, consequently, a larger torque.

This phase-dependent behavior provides a route toward an active optomechanical switch operating between low- and high-torque states. Switching may be induced by thermal or electrical stimulation of the PCM, without requiring a continuous external voltage bias to maintain its material phase.

From a fundamental physics perspective, this study shows that optical heterogeneity, combined with an asymmetric rotational geometry, can generate a substantial net Casimir torque without intrinsic material anisotropy. This provides a useful physical concept for designing tunable micro- and nanoelectromechanical devices. These results build on previous studies of Casimir-force modulation using phase-change materials [3, 4], while extending the concept to torque generation in a heterogeneous rotational system.

Related torsional PCM-MEMS work also addresses phase-dependent thermal effects [12].

A normalized angle close to unity represents proximity to contact, even though the physical angle remains small. The Taylor expansion of the torque requires $|\phi| \ll 1$ and should not be extrapolated to this regime. The validity of the local proximity approximation is a separate issue involving the gap, slope, finite plate dimensions, and coating boundary. Near contact, the results can also become more sensitive to surface roughness and the material description at small separations.

Another potentially important extension would be to incorporate surface roughness into the theoretical model. At very small separations, local variations in the gap can significantly modify the electromagnetic interaction. Including experimentally realistic roughness profiles would therefore provide a more comprehensive assessment of the robustness of the predicted Casimir torque. Finite-size and edge effects also warrant further investigation.

Combining phase-change materials, heterogeneous surface coatings, and rotational geometry provides a means to actively tune the Casimir torque. The proposed configuration allows adjustment of both the torque amplitude, through switching between weak- and strong-torque regimes, and the thermal response, through switching between relatively temperature-insensitive and temperature-responsive regimes. These characteristics highlight the potential of phase-change-enabled Casimir systems for tunable optomechanical switching, thermal sensing, and low-power NEMS applications.

References

1. H. B. G. Casimir, "On the attraction between two perfectly conducting plates," Proceedings of the Koninklijke Nederlandse Akademie van Wetenschappen **51**, 793–795 (1948).
2. F. M. Serry, D. Walliser, and G. J. Maclay, "The role of the Casimir effect in the static deflection and stiction of membrane strips in microelectromechanical systems (MEMS)," Journal of Applied Physics **84**, 2501–2506 (1998). doi:10.1063/1.368410.
3. G. Torricelli, P. J. van Zwol, O. Shpak, C. Binns, G. Palasantzas, B. J. Kooi, V. B. Svetovoy, and M. Wuttig, "Switching Casimir forces with phase-change materials," Physical Review A **82**, 010101(R) (2010). doi:10.1103/PhysRevA.82.010101.
4. M. Sedighi, W. H. Broer, S. Van der Veeke, V. B. Svetovoy, and G. Palasantzas, "Influence of materials' optical response on actuation dynamics by Casimir forces," Journal of Physics: Condensed Matter **27**, 214014 (2015). doi:10.1088/0953-8984/27/21/214014.
5. E. M. Lifshitz, "The theory of molecular attractive forces between solids," Soviet Physics JETP **2**, 73–83 (1956).
6. B. E. Sernelius, "Different Approaches," in *Fundamentals of van der Waals and Casimir Interactions*, Springer Series on Atomic, Optical, and Plasma Physics, Vol. 102 (Springer, Cham, 2018), pp. 109–123. doi:10.1007/978-3-319-99831-2_6.
7. F. Tajik, *Casimir Torques and Lateral Forces: Influence of Optical Properties and Surface Morphology*, Ph.D. thesis, University of Groningen (2018). University repository.
8. B. Spreng, T. Gong, and J. N. Munday, "Recent developments on the Casimir torque," International Journal of Modern Physics A **37**, 2241011 (2022). doi:10.1142/S0217751X22410111.
9. B. Elsaka, X. Yang, P. Kästner, K. Dingel, B. Sick, P. Lehmann, S. Y. Buhmann, and H. Hillmer, "Casimir Effect in MEMS: Materials, Geometries, and Metrologies—A Review," Materials **17**, 3393 (2024). doi:10.3390/ma17143393.
10. M. Dhital and U. Mohideen, "A Brief Review of Some Recent Precision Casimir Force Measurements," Physics **6**, 891–904 (2024). doi:10.3390/physics6020055.
11. B. Spreng and J. N. Munday, "Thermal Effects in the Casimir Torque between Birefringent Plates," Physical Review Letters **135**, 013602 (2025). doi:10.1103/32gq-dbms.

12. F. Tajik and Z. Dadigiv, “Chaotic motion due to amorphous to crystalline phase transition in torsional Casimir MEMS under the influence of thermal fluctuations,” Physica B: Condensed Matter **718**, 417881 (2025). doi:10.1016/j.physb.2025.417881.